Journal of Computer-Aided Molecular Design **17:** 713–724, 2003.

Thermodynamic conformational analysis and structural stability of the nicotinic analgesic ABT-594

M. Mora, C. Muñoz-Caro & A. Niño*
Grupo de Química Computacional, E.S. Informática, Universidad de Castilla-La Mancha, Paseo de la Universidad 4, E-13071 Ciudad Real, Spain

Received 3 April 2003; accepted in revised form 2 October 2003

Key words: ABT-594, conformational population, internitrogen separation, nicotinic analgesic, nicotinic pharmacophore

Summary

This work presents a theoretical study of the nicotinic analgesic ABT-594. We describe its neutral (precursor) and protonated (active) forms in vacuum and aqueous solution at the MP2/cc-pVDZ level. A conformational analysis is performed on the two torsional angles describing the orientation of the azetidinyl group and the azetidinylmethoxy moiety. To account for entropic effects, a thermostatistical study of conformational populations at physiological temperature is carried out. In the neutral form, conformer I is found as the most populated in vacuum and solution. Here, the nitrogen of the azetidinyl group is far from the electron pairs of the oxygen and the pyridinic nitrogen. In the protonated form, conformer VIII is the most stable in vacuum and solution. Now, the additional proton on the azetidinyl group is oriented toward the electron lone pairs of oxygen. The structural stability of conformers I and VIII is considered through the atoms in molecules theory. The conformer I, in the neutral forms, is stabilized by an intramolecular hydrogen bond. The preference of conformer VIII in the protonated forms is explained by the higher strength of its intramolecular hydrogen bond over the cation-π interaction found in conformer I. The effect of the interaction energy with the receptor on the conformational preferences of protonated ABT-594 is simulated. The result is that the population of conformers associated to the rotation of the azetidinyl group increases. So, the molecule can easily adopt the optimal internitrogen separation for interaction with the receptor.

Introduction

Current analgesics in use fall mainly in one of two classes, opiod analgesics and Non-Steroidal Anti-Inflammatory Drugs (NSAIDs) [1]. These compounds are extensively used in the treatment of pain, but they exhibit some unwanted side effects. Thus, opioids produce physical addiction, respiratory depression and constipation, among other undesirable effects [1]. On the other hand, inspecificity of present NSAIDs for the COX-1 and COX-2 isoforms of the cyclooxygenase enzyme is translated in gastric irritation and renal dysfunction, apart from its analgesic and anti-inflammatory activity [1, 2]. For these reasons, it is of great interest to develop new approaches to the treatment of pain, free from the side effects mentioned above.

The antinociceptive power of nicotine was reported as early as 1932 [3]. However, nicotine has not been developed as an analgesic agent due to its weak analgesic activity and its profile of side effects. The present interest in the nicotinic mechanism, as an alternative route to pain management, dates from 1976 when John Daly identified in the skin of the Ecuadorian frog *Epipedobates Tricolor* a compound 200 times more potent than morphine at blocking pain in animals [4–5]. The active principle was called epibatidine, and it was shown to exert its analgesic activity by acting on the nicotinic acetylcholine receptor (nAChR) [4, 6]. The structure of epibatidine was not elucidated until the 1990s [7]. Despite its great activity, the lack of

*To whom correspondence should be addressed. E-mail: quimcom@uclm.es

specificity of epibatidine on the different subtypes of nicotinic receptors results in an important profile of side effects on the respiratory, gastrointestinal and cardiovascular functions [8]. Therefore, epibatidine is not used as an analgesic agent, but represents an important tool in the study of the function of the nAChR.

The nicotinic receptor, the target of nicotinic analgesics, is a kind of ligand gated ion channel, where acetylcholine is the endogenous ligand [9]. This receptor is a transmembrane protein with the ligand receptor site placed at the extracellular side. The first model of nicotinic pharmacophore was proposed by Beers and Reich [10] and refined by Sheridan and coworkers [11]. Following this model, the nicotinic pharmacophore comprises a basic nitrogen (a centre of charge) and a hydrogen bond acceptor. The optimal distance proposed in this model between the charge centre and the hydrogen bond acceptor is 4.8 Å. Posterior studies on epibatidine found an internitrogen separation of 5.5 Å [12]. Additional studies, using molecular mechanics optimized geometries for epibatidine and related compounds, found internitrogen distances as long as 6.1 Å [13]. These data show that the question of the role played by the internitrogen separation in the nicotinic pharmacophore remains unanswered; for a review see [14].

Several compounds structurally related to epibatidine and exhibiting analgesic activity have been developed to date [15]. Among them, the compound called ABT-594, (R)-5-(2-azetidinylmethoxy)-2-chloropyridine [16, 17], is equal in efficacy to morphine across a series of diverse animal models of acute thermal, persistent chemical, and neuropathic pain states [17]. In addition, repeated treatment with ABT-594 does not seem to elicit opioid-like withdrawal or physical dependence [17]. It has been shown that ABT-594 is much less toxic than epibatidine due to its higher selectivity for the nAChR of the central nervous system (CNS) [16]. Similarly to epibatidine, ABT-594 shows a lack of stereoselectivity at its binding to the nAChR of the CNS, with the S-enantiomer (called A-98593) being more potent at the neuromuscular nAChR [18]. At present, ABT-594 is in clinical Phase II [15]. For these reasons, ABT-594 can be considered the starting point of a new generation of potent nicotinic analgesics.

Despite the interest of ABT-594, to our knowledge no theoretical treatment of the properties of this compound has been carried out. Considering the existence of a basic nitrogen in the azetidinyl moiety of ABT-594, at physiological pH we have the neutral (precursor) form in equilibrium with the protonated (active) form. As illustrated in [19] for aminopyridines, the study of the neutral and protonated ligand is needed for any model of activity that expresses thermostatistically the protonation equilibrium and the binding constant with the receptor.

As the starting point toward the development of a model of activity for nicotinic analgesics, we present here the first theoretical characterization of the conformational behaviour of ABT-594. Thus, its neutral (precursor) and protonated (active) forms are considered, both in vacuum and aqueous solution. To account for the influence of entropic effects, the most stable conformations are determined at physiological temperature, in thermostatistical rather than on pure energetic terms. In addition, the effect of the interaction (binding) energy on the conformational equilibria is also simulated. For the more stable conformations found, an Atoms in Molecules (AIM) study is performed to characterize the observed structural stability.

Methodology

To describe the conformational behaviour of ABT-594, ab initio methodology has been applied including correlation energy at the MP2 level. As basis set, we have used the correlation consistent, double-zeta, cc-pVDZ basis set [20], which includes by definition polarization functions on hydrogen and heavy atoms. All the geometry optimizations are carried out using the quasi-Newton BERNY algorithm [21].

To have a realistic description of the molecular behaviour in aqueous solution (dielectric constant, $\varepsilon = 78.39$) the solvent effect is described using the Polarizable Continuum Model (PCM) [22, 23]. In this approach, a van der Waals surface cavity is used, as well as a detailed description of the electrostatic potential. The cavity/dispersion contribution is parameterized considering the surface area. The PCM model performs a realistic description of the molecular shape. All the calculations are carried out using the Gaussian 98 package [24].

The structure and numbering convention for ABT-594 (in neutral and protonated form) are shown in Figure 1. The conformational flexibility is accounted for considering three dihedral angles, θ_1, θ_2 and τ. θ_1 measures the torsion of the azetidinylmethoxy moiety. θ_2 describes the rotation of the azetidinyl group. Finally, τ defines the orientation of the oxy-

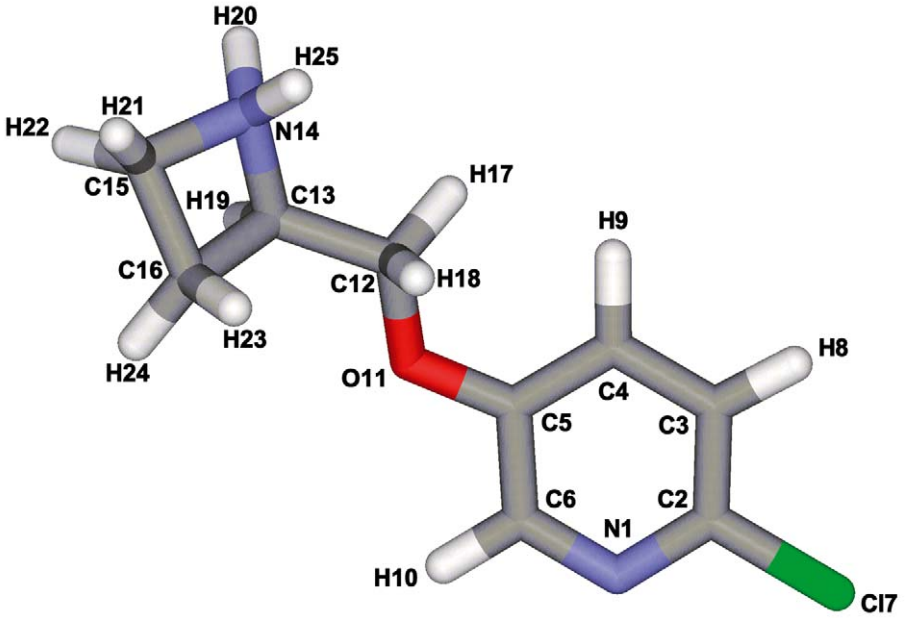

Figure 1. Structure and numbering convention of ABT-594 used in this work. The protonated form is shown. The neutral form lacks H25. The atoms' colour code is as follows: grey: carbon; blue: nitrogen; red: oxygen; green: chlorine; white: hydrogen.

gen lone pairs. Using the numbering of Figure 1, the θ_1, θ_2 and τ torsional angles are defined as dihedrals C13C12O11C5, N14C13C12O11, and C12O11C5C4, respectively. For reasons described below, our conformational analysis focuses on the variation of θ_1 and θ_2 with τ restricted to values near 0° (though fully optimized for each θ_1, θ_2 pair).

For the θ_1 and θ_2 angles, the positive sense of rotation is defined as clockwise, with C5 (or O11) placed closer to the observer and looking through the O11-C12 (or C12-C13) axis. A potential energy hypersurface is defined from a grid of points in θ_1 and θ_2. This grid is obtained considering a range from 0° to 360° using increments of 60° for each angle. In vacuum, all the grid points have been fully optimized. From the grid, the local minima are identified and localized by full relaxation of the closer structures. The algorithmic limitations of the software employed force us to freeze the geometries for the solvated molecules at the values optimized in vacuum.

To take into account not only enthalpic but also entropic effects in the stability of the conformers we apply statistical thermodynamics. Thus, the original grid of energetic data is transformed in a detailed grid of values (100 × 100 points) placed at equal increments of the θ_1 and θ_2 large amplitude coordinates. This detailed hypersurface is derived from the original one applying the Kriging interpolation method [25] with the Surfer 8 package [26]. Kriging is a form of weighted averaging where the weights are chosen in such a way that they minimize the estimation variance. From the energy data, we build a conformational partition function. As described in [27], we build the conformational partition function, Q_c, at temperature T, from the energy hypersurface, $E(\theta_1, \theta_2)$, by considering a Boltzmann distribution:

$$Q_c = \int_{\theta_1}\int_{\theta_2} \exp[-E(\theta_1, \theta_2)/kT]d\theta_1 d\theta_2, \qquad (1)$$

where k represents the Boltzmann constant.

The double integral in Equation 1 is numerically evaluated using a bicubic spline [28] as:

$$Q_c = \sum_{i}^{\theta_1}\sum_{j}^{\theta_2}\sum_{l=0}^{3}\sum_{m=0}^{3} a_{ijlm} \frac{(\theta_1(i+1) - \theta_1(i))^{l+1}}{l+1} \frac{(\theta_2(j+1) - \theta_2(i))^{m+1}}{m+1}, \qquad (2)$$

where the first two summations represent the grid of points in the θ_1 and θ_2 coordinates. The a_{ijlm} are the coefficients of the spline obtained from the energy hypersurface, $E(\theta_1, \theta_2)$. As detailed in [28], the spline, S, fulfills the interpolation condition, $S(\theta_1, \theta_2)$=$E(\theta_1, \theta_2)$, for all the grid data points. In

Table 1. Values of the θ_1, θ_2, and τ dihedrals, and energy difference, ΔE, for the most open structures of neutral and protonated ABT-594. Fully optimized geometries. Angles in degrees and energy in kJ mol^{-1}.

Form	θ_1	θ_2	τ	ΔE
Neutral[a]	180.4	172.1	179.7	0.0
Neutral[b]	180.6	171.8	359.2	1.1
Protonated[a]	180.3	168.1	180.9	0.0
Protonated[b]	180.2	167.5	0.1	3.7

[a]Electron lone pairs of O11 and N1 in antieclipsed conformation.
[b]Electron lone pairs of O11 and N1 in eclipsed conformation.

addition, S is continuously differentiable in $E(\theta_1, \theta_2)$, and $\partial^2 S/\partial\theta_1\partial\theta_2$ is continuous in $E(\theta_1, \theta_2)$.

The conformational population, p, for given θ_1, θ_2 values is determined from Q_c as

$$p(\theta_1, \theta_2) = \exp[-E(\theta_1, \theta_2)/kT]/Q_c. \quad (3)$$

To account for the overall population in a given interval delimited by the values θ_1(i), θ_2(i), θ_1(j), θ_2(j) we compute the double integral,

$$p(\Delta\theta_1, \Delta\theta_2) = \int_{\theta_1(i)}^{\theta_1(j)} \int_{\theta_2(i)}^{\theta_2(j)} p(\theta_1, \theta_2) d\theta_1 d\theta_2 \quad (4)$$

performing the numerical integration of a bicubic spline derived from $p(\theta_1, \theta_2)$. Equations 2–4 are evaluated using software developed at our laboratory that incorporates the numerical routines provided in [28].

To characterize the most stable structures, the AIM theory is applied by means of the package Morphy98 [29]. In all cases (neutral and protonated forms, in vacuum and solution), the AIM theory is applied from the corresponding one-determinantal electronic density functions.

Results and discussion

Structural results

As shown in Figure 1, conjugation of O11 with the pyridinic ring can appear for τ values close to 0° and 180°. In these conformations the electron lone pairs of oxygen are placed above and below the pyridinic ring plane, maximizing the overlap with the pyridinic π-system. To test the difference in energetic terms between the two possibilities, we have fully optimized the conformations with starting θ_1 and θ_2 values of 180° (the most open structure) and τ values of 0° and 180°. The calculation has been performed for the neutral and the protonated forms. Table 1 collects the results after full relaxation of the geometry. We observed that the initial θ_1, θ_2, and τ values change slightly during the optimization. The energy difference between conformers starting at $\tau = 0°$ and 180° are 1.1 and 3.7 kJ mol^{-1}, for the neutral and protonated compounds, respectively. In both cases the most stable conformer corresponds to $\tau \approx 180°$. This is a conformation where the electron lone pairs of O11 and N1 are placed in antieclipsed form. Thus, electronic repulsion is minimized, although the difference in energy (less than 1 kcal mol^{-1}) is too small to define a structurally preferred conformation.

These results suggest that on energetic grounds there is no clearly preferred conformation with respect to the τ angle. Comparison with other nicotinic agonists will be useful to clarify this question. Thus, DBO-83, a 3,8-diazabicyclo[3.2.1]octane derivative, exhibits morphine-like analgesic potency and efficacy [30]. This compound shows selectivity for the neuronal nAChR [30], as well as ABT-594 does. In DBO-83, an azo group is part of the aromatic ring. Thus, there is an additional nitrogen in sp^2 hybridization next to what could be considered the pyridinic nitrogen in ABT-594. In other words, we have the two electron lone pairs from the nitrogens eclipsing each other. Also, the compound known as RJR-2403 [(E)-N-methyl-4-(3-pyridinyl)-3-butene-1-amine] shows specificity for the neuronal nAChR [31]. RJR-2403 has a double bond between two carbon atoms in a relative position, to the pyridinic ring, equivalent to the oxygen atom in ABT-594. These data suggest that selectivity for the neuronal nAChR is associated with the presence of an electronegative zone oriented in the same direction as the electron lone pair of the electronegative atom involved in the putative hydrogen bond with the receptor site. For these reasons, we assign an initial value of $\tau = 0°$ (in which the O11 and N1 electron pairs eclipse each other), and perform the full conformational analysis on θ_1 and θ_2.

Figure 2 shows the fully relaxed two-dimensional energy hypersurfaces obtained for the neutral and protonated ABT-594 in vacuum. We can observe the existence of a quasi-threefold symmetry on the θ_1 and θ_2 coordinates. This fact results in nine possible minima in the hypersurface, on θ_1 and θ_2. These minima correspond to θ_1 and θ_2 values close to 60°, 180° and 300°. Taking into account the different θ_1, θ_2 couples, we define the conformers of minimal energy as: I (60°,

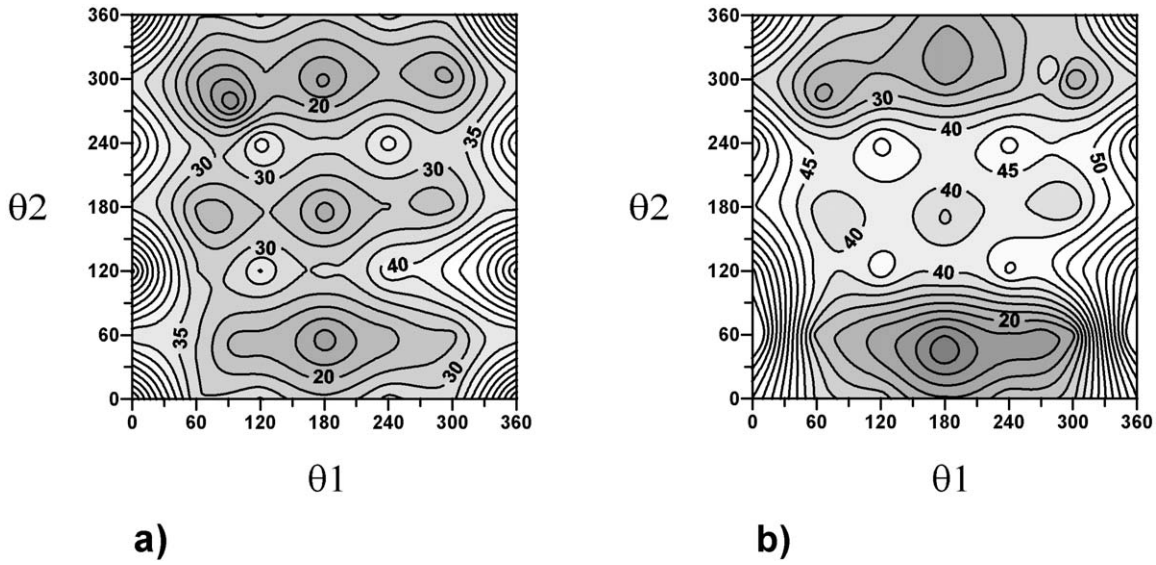

Figure 2. Potential energy hypersurfaces, in vacuum, of neutral (case a) and protonated (case b) ABT-594 for the torsional motion around the θ_1 and θ_2 dihedral angles. Interval between isocontour lines 5 kJ mol^{-1}. Angles in degrees. Darker zones correspond to lower energy zones.

Table 2. θ_1 and θ_2 values (in degrees) and energy increments (in kJ mol^{-1}) in vacuum for the different minima located on the conformational energy hypersurfaces of neutral and protonated ABT-594. Energetic data refer to the global minimum for each species.

Conformer	θ_1[a]	θ_2[a]	ΔE[a]	θ_1[b]	θ_2[b]	ΔE[b]
I	93.1	277.0	0.0	64.4	283.7	17.0
II	177.8	296.1	8.5	181.8	309.0	16.7
III	292.1	306.3	13.4	281.2	308.4	39.7
IV	78.2	168.3	15.1	78.3	167.3	34.7
V	180.6	171.8	12.4	180.2	167.5	34.0
VI	279.5	181.9	21.9	288.2	184.8	34.9
VII	97.2	51.8	17.3	–	–	–
VIII	180.4	53.6	7.3	178.7	43.8	0.0
IX	–	–	–	271.2	58.2	11.6

[a]Neutral form.
[b]Protonated form.

300°), II (180°, 300°), III (300°, 300°), IV (60°, 180°), V (180°, 180°), VI (300°, 180°), VII (60°, 60°), VIII (180°, 60°) and IX (300°, 60°). Their specific locations (after full relaxation of the geometry) for the neutral and protonated forms in vacuum are collected in Table 2. Figure 2 shows that the energy minima are organized in three zones for θ_2 values about 60°, 180° and 300°. These zones are separated from each other by two zones of local maxima, for θ_2 values close to 120° and 240°.

As shown in Table 2, the global minimum in the neutral form is found, in vacuum, for conformer I, at $\theta_1 = 93.1°$, $\theta_2 = 277.0°$. Close in energy, less than 9 kJ mol^{-1} (2.1 kcal mol^{-1}), we found conformers II and VIII, see Table 2. Conformer VIII is the closer one, placed at only 7.3 kJ mol^{-1} from the absolute minimum. Figure 2 shows that the maximum energy separating conformers I and II is about 20 kJ mol^{-1} (4.8 kcal mol^{-1}). The high energy zones separating the minima, at θ_2 values close to 240° and 120°, reach 35–40 kJ mol^{-1} in height. These barriers separate conformers (I, II, III) from (IV, V, VI) and (IV, V, VI) from (VII, VIII, IX), respectively.

For the protonated form in vacuum, Figure 2 shows that conformer VIII becomes the global minimum. Table 2 shows that the closest local minimum, 11.6 kJ mol^{-1} (2.8 kcal mol^{-1}), corresponds to conformer IX. In addition, the high energy barriers reach 50–55 kJ mol^{-1} for θ_2 values close to 240°, and 50 kJ mol^{-1} for θ_2 values about 120°. Therefore, on protonation, the conformational preference of ABT-594 experiences a large change. In addition, the protonated form seems to exhibit less conformational flexibility than the neutral one. However, this last point is difficult to quantify on pure energetic grounds.

Figure 3 shows the two-dimensional energy hypersurfaces obtained for the neutral and protonated ABT-594 in aqueous solution, using the geometries fully relaxed in vacuum. Table 3 collects the energy values obtained in solution at the minima found in

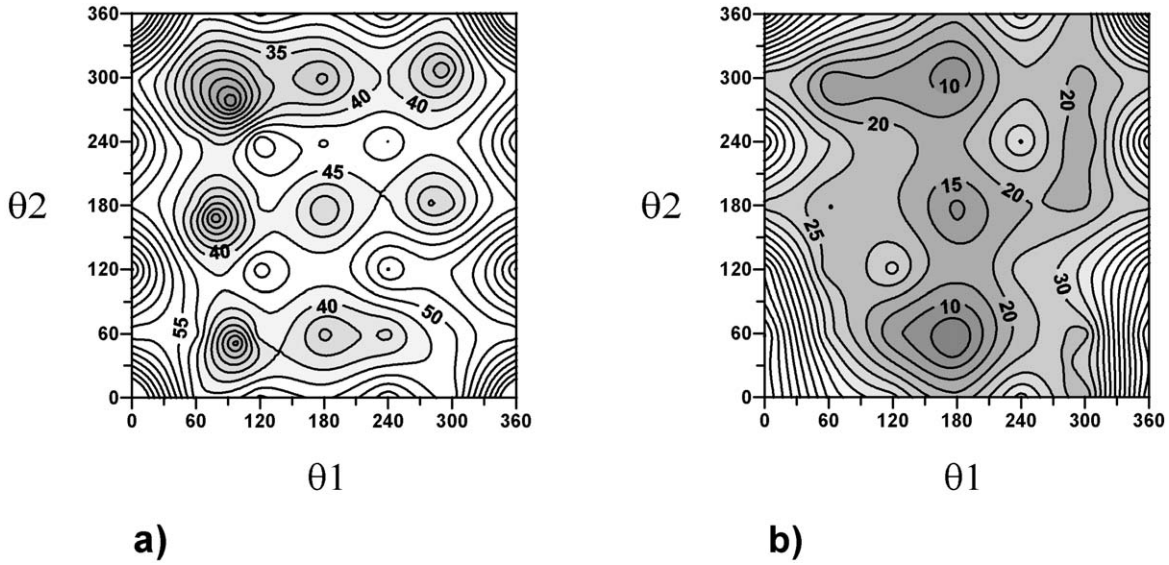

Figure 3. Potential energy hypersurfaces, in aqueous solution, of neutral (case a) and protonated (case b) ABT-594 for the torsional motion around the θ_1 and θ_2 dihedral angles. Interval between isocontour lines 5 kJ mol^{-1}. Angles in degrees. Darker zones correspond to lower energy zones.

Table 3. θ_1 and θ_2 values (in degrees) and energy increments (in kJ mol^{-1}) in aqueous solution for the different minima located on the conformational energy hypersurfaces of neutral and protonated ABT-594 in vacuum. Energetic data refer to the global minimum for each species.

Conformer	θ_1[a]	θ_2[a]	ΔE[a]	θ_1[b]	θ_2[b]	ΔE[b]
I	93.1	277.0	0.0	64.4	283.7	11.9
II	177.8	296.1	23.9	181.8	309.0	6.8
III	292.1	306.3	20.2	281.2	308.4	21.0
IV	78.2	168.3	10.6	78.3	167.3	21.7
V	180.6	171.8	30.2	180.2	167.5	9.7
VI	279.5	181.9	28.9	288.2	184.8	18.0
VII	97.2	51.8	12.1	–	–	–
VIII	180.4	53.6	30.0	178.7	43.8	1.6[c]
IX	–	–	–	271.2	58.2	27.0

[a]Neutral form.
[b]Protonated form.
[c]The minimum is found at $\theta_1 = 180°$, $\theta_2 = 60°$.

vacuum. Due to the lack of geometry relaxation, the present results have only a qualitative meaning.

For the neutral form in solution, Table 3 shows that conformer I is still the most stable species. In addition, conformers IV and VII decrease in energy, whereas conformers II, III, V, VI and VIII experience an increase. The high energy zones around $\theta_2 = 240°$ and $\theta_2 = 120°$ increase in energy, reaching 55–60 kJ mol^{-1}. Figure 3 shows that the maxima of energy for interconversion between the couples of conformers (I, II), (II, III), (IV, V), (V, VI) and (VII, VIII) also increase. Thus, in solution, higher energy barriers must be overcome to interconvert between the conformers of neutral ABT-594.

As expected, the protonated form exhibits the largest change in solution. The energy minimum is found at the VIII conformer. As seen in Figure 3, we have a zone of three close minima for $\theta_1 \approx 180°$ (conformers II, V, VIII), which interconvert as a function of θ_2. This behaviour represents an inversion with respect to that observed in all other cases, where the closest minima interconvert as a function of θ_1. Tables 2 and 3 show that in solution all the conformers experience a decrease in energy, except conformer IX that increases from 11.6 to 27.0 kJ mol^{-1}. The global minimum is again found for conformer VIII, with θ_1, θ_2 values of 180°, 60°, respectively. Thus, the minimum is slightly displaced from the placement in vacuum. Isoforms II and V are close to the minimum, placed at 6.8 and 9.7 kJ mol^{-1}, respectively. The high energy zone between conformers (II, V) and (V, VIII) reaches 15–20 kJ mol^{-1}. Comparison of Figures 2 and 3 shows that the energy hypersurface for the protonated form, in solution, is flatter than in vacuum. All these data indicate that the protonated (active) form in solution is more flexible, in energetic terms, than in vacuum. In particular, rotation on the θ_2 dihedral (rotation of

the azetidinyl head) is favoured, whereas the θ_1 angle remains close to 180°.

Structural stability of conformers

To characterize the reasons for the different stabilities of the reference conformers I and VIII (for neutral and protonated forms, in vacuum and solution), we resort to the Atoms In Molecules (AIM) theory. The AIM theory characterizes a bond by an atomic interaction line (AIL) [32, 33]. An AIL is a path through the electron density, ρ, along which ρ is a maximum with respect to any neighbouring point. On the AIL lies the bond critical point (BCP), a second order saddle point where ρ reaches a minimum [32, 33]. The value of the electronic density at the BCP for a given bond, ρ_b, is correlated to the concept of bond order [33]. Thus, higher values of ρ_b correspond to higher degrees of conjugation and stronger bonds. In addition, the sign of the Laplacian of the charge density at the BCP, $\nabla^2\rho_b$, defines the interaction responsible for the bonding [32, 33]. A negative sign corresponds to a shared interaction, where the electronic charge is shared by the two nuclei. This is the case for covalent bonds. A positive sign corresponds to a closed-shell interaction, where the electronic charge is concentrated near each nucleus. This is the case for ionic and hydrogen bonds.

We have applied the AIM theory to conformers I and VIII in the neutral and protonated forms in vacuum and solution. The geometry fully optimised in vacuum is always used. For all the BCP, the AIL has been traced to identify unambiguously the bonded atoms. After computing the BCP points and its $\nabla^2\rho_b$ values, we observe the existence of non covalent bonds ($\nabla^2\rho_b > 0$). No variation is found when going from vacuum to solution. Figure 4 collects the structure of conformers I and VIII in neutral and protonated forms, as well as the non covalent bonds identified.

We find that for neutral ABT-594, in vacuum and solution, conformer I is stabilized by an intramolecular hydrogen bond. This bond involves the azetidinyl moiety (N14) and a hydrogen (H9) of one carbon on the aromatic ring (C4), see Figure 1 and case (a) of Figure 4. Similar orientations of the pyrrolidine nitrogen and pyridine hydrogens are found in nicotine [34]. When protonated, in vacuum and solution, the conformer I is stabilized by a bond involving the azetidinyl nitrogen (N14) and one carbon (C6) on the aromatic pyridinic ring, see case (c) of Figure 4. Thus, we have an interaction between the positively charged head and the aromatic ring. This suggests a typical cation-π interaction. In fact, the positive $\nabla^2\rho_b$ value (0.039 a.u.) shows that this is a closed-shell interaction, as a cation-π interaction is. In addition, the ρ_b value is 0.011 a.u. These data agree with the values for ρ_b and $\nabla^2\rho_b$ found for the cation-π interaction of protonated aminopyridines with an ethylene group [35].

With respect to conformer VIII, it is always stabilized by an intramolecular hydrogen bond. In the neutral forms, vacuum and solution, the bond involves the oxygen atom (O11) and a hydrogen (H21) on carbon C15 (one carbon of the azetidinyl moiety), see case (b) of Figure 4. In contrast, for the protonated forms, vacuum and solution, the hydrogen bond involves the oxygen (O11) and one hydrogen (H25) on the azetidinyl nitrogen, see case (d) of Figure 4.

ρ_b can be used as an index of bond order, but direct comparison of bond strengths between different pairs of atoms using their ρ_b value is not correct [33]. Anyway, the exponential dependence of the bond order on ρ_b suggests that for neutral ABT-594 the N14H9 bond in conformer I is stronger than the O11H21 bond in conformer VIII (ρ_b values of 0.017 a.u. and 0.009 a.u., respectively). Additional information can be gained by comparison with the OH hydrogen bond in the methanal–water complex, which is weak (35 kJ mol^{-1}) and has a ρ_b of 0.018 a.u. [32]. This datum indicates that our $\rho_b = 0.009$ a.u. for the O11H21 bond in conformer VIII corresponds in fact to a very weak hydrogen bond. This explains the higher stability of conformer I in the neutral molecule. On the other hand, in the protonated ABT-594, the N14C6 cation-π interaction in conformer I is characterized by a ρ_b value of 0.011 a.u. In turn, the H25O11 hydrogen bond in conformer VIII exhibits a ρ_b value of 0.023 a.u. This hydrogen bond is, then, very much stronger than the O11H21 bond found in the neutral form, and than the hydrogen bond in the methanal–water complex. However, we cannot directly conclude that the N14C6 bond is weaker than the H25O11 one. We can get some insight of the strength of the N14C6 cation-π interaction comparing with the binding energy of some known cation-π complexes. Experimental measurements yield a binding energy of 9.4 kcal mol^{-1} for the N(Methyl)$_4^+$-C_6H_6 cation-π complex [36]. This binding energy is comparable to the OH hydrogen bond energy previously quoted for the methanal–water complex (35 kJ mol^{-1}). Since the present H25O11 hydrogen bond has a ρ_b value of 0.023 a.u., it is much stronger than the OH hydrogen bond in the methanal–water complex, with $\rho_b =$

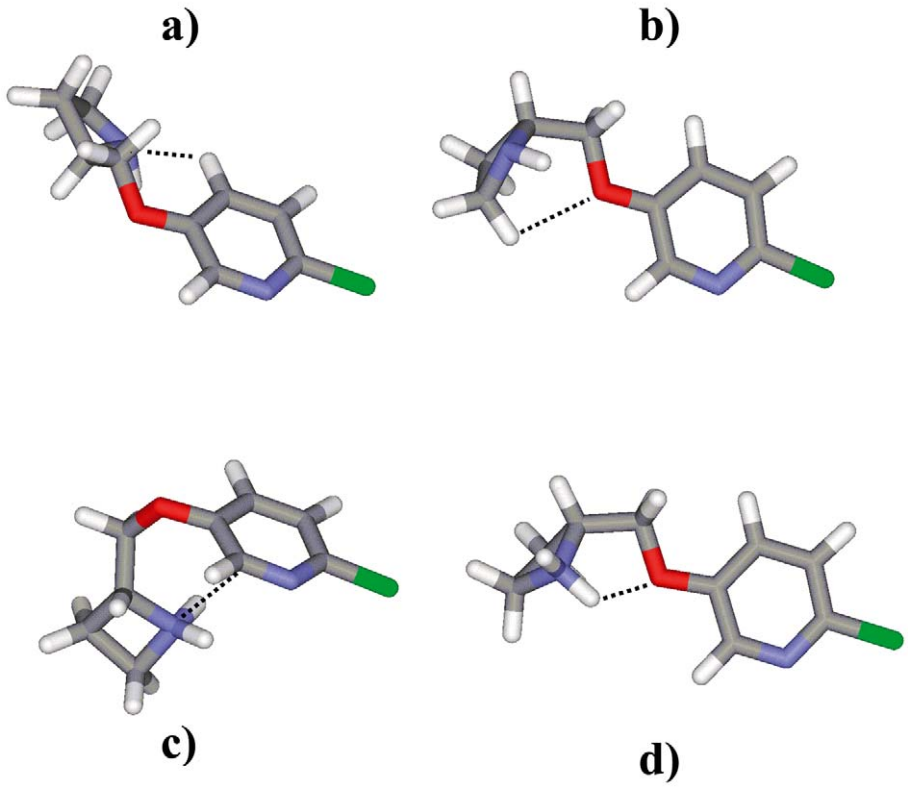

Figure 4. Structure of the preferred conformers found for neutral and protonated ABT-594. Geometries optimized in vacuum. The dotted lines represent the non-covalent bonds found. Case (a) conformer I in the neutral form. Dotted line: N14H9 hydrogen bond. Case (b) conformer VIII in the neutral form. Dotted line: O11H21 hydrogen bond. Case (c) conformer I in the protonated form. Dotted line: N14C6 cation-π bond. Case (d) conformer VIII in the protonated form. Dotted line: O11H25 hydrogen bond. The atoms' colour code is as follows: grey: carbon; blue: nitrogen; red: oxygen; green: chlorine; white: hydrogen.

0.018 a.u. It is then reasonable to conclude that the H25O11 hydrogen bond is stronger than the N14C6 cation-π interaction. This fact explains the preference of conformer VIII when ABT-594 is protonated.

Thermodynamic stability of conformers

Purely energetic (enthalpic) criteria are not a good index for the stability of conformers, since entropic effects are absent. Thus, to quantify the relative population of the different conformers at physiological temperature (37 °C), the conformational partition function was computed. A population analysis was performed as indicated in the Methodology section. Figures 5 and 6 show the population maps for the neutral and protonated forms, in vacuum and solution. To account quantitatively for the population of each isoform, we have evaluated the volume under each peak in Figures 5 and 6, by integrating a bicubic spline as a function of θ_1 and θ_2. Since the base value of population in the population maps is 10^{-6}–10^{-8}, we select as limits of integration for each peak the zone delimited by a population value of 10^{-6}, as minimum. When two peaks are so close that the population between them is higher than 10^{-6}, we define the limit for integration in the minimum of population connecting the peaks. Table 4 collects the population values for the different conformers found in Figures 5 and 6.

Figure 5 and Table 4 show that in vacuum in the neutral form conformer I is the most populated isoform. This isoform is followed by conformers VIII, II, V and III with a much smaller population. For the protonated form, the only significantly populated isoforms are conformers VIII and IX. We see (Table 4) that for the neutral form, isoform I has the highest weight (65.6%). Conformations II and VIII are much less populated, but in similar amounts, 9.0% and 16.3%, respectively. Conformers V and III have a small population ($\leq$1.3%). On protonation, isoform VIII is dominant (95.8%). The small contribution from

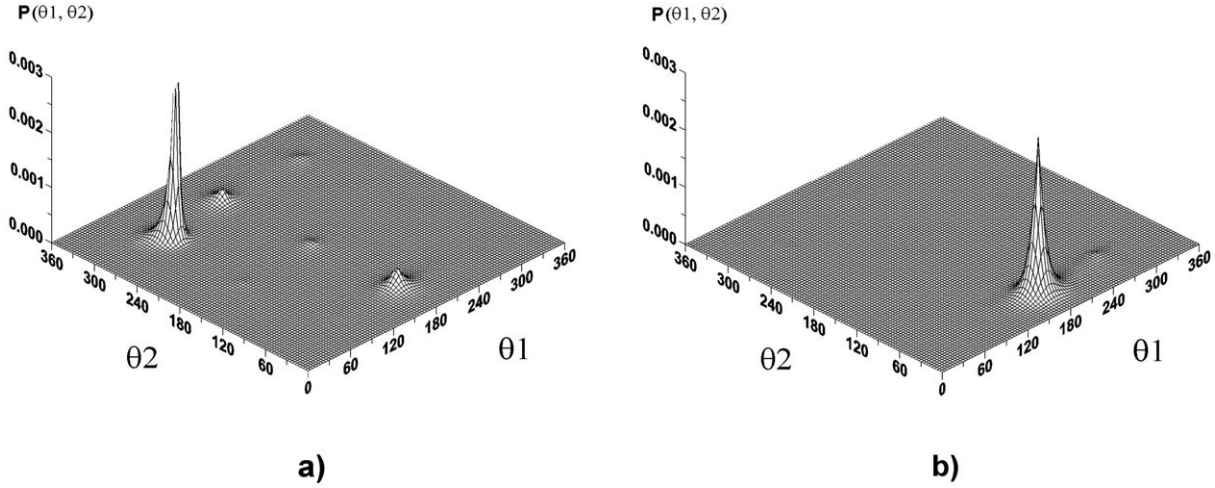

Figure 5. Wireframe map of conformational populations for neutral (case a), and protonated (case b) ABT-594 in vacuum at physiological temperature (37 °C). Angles in degrees.

Table 4. Population (in per cent) of the significantly populated conformers of the neutral and protonated ABT-594 in vacuum and aqueous solution. Data at physiological temperature (37 °C).

Conformer	Case[a]	Case[b]	Case[c]	Case[d]
I	65.6	–	97.8	–
II	9.0	–	–	10.1
III	1.1	–	–	–
IV	–	–	1.1	–
V	1.3	–	–	2.9
VIII	16.3	95.8	–	80.4
IX	–	2.4	–	–

[a]Neutral ABT-594 in vacuum.
[b]Protonated ABT-594 in vacuum.
[c]Neutral ABT-594 in solution.
[d]Protonated ABT-594 in solution.

isoform IX (2.4%) is almost merged with isoform VIII.

In solution, see Figure 6 and Table 4, the neutral form is essentially found in the isoform I (97.8%) with a very small contribution of conformer IV (1.1%). Thus, accessibility of conformations is reduced with respect to vacuum. On the other hand, Table 4 shows that in solution conformer VIII is the most populated, as in vacuum, but the population is reduced from 95.8% to 80.4%. In addition, several conformers are now significantly populated: isoforms II and V. Isoform II is populated in 10.1%, followed by isoform V with 2.9%. As seen in Figure 3, case (b), isoforms II and VIII are separated by a barrier, placed at $\theta_2 = 0°$ (360°), of 25 kJ mol^{-1} (5.9 kcal mol^{-1}) when going from isoformVIII to II. The barrier is about 13 kJ mol^{-1} (3.1 kcal mol^{-1}) if going from II to VIII. Thus, isoforms II and VIII interconvert by a torsion of the azetidinyl moiety. These results indicate that conformer VIII (and conformer II, which is structurally equivalent by a torsion on θ_2) is the form existing in solution at physiological temperature.

The three-dimensional structures of the thermodynamically most stable conformers for neutral (isoform I) and protonated (isoform VIII) ABT-594 are collected in cases (a) and (d) of Figure 4. The fundamental difference between the two structures is that the charged nitrogen in the protonated form is closer to the electron pairs of oxygen, oriented toward the pyridinic nitrogen.

Internitrogen separation

The distance between the two nitrogens, r_{NN}, in the protonated form is of interest since it is one factor defining the 3D nicotinic pharmacophore [10–13]. Different values have been given for r_{NN} in several studies using different nicotinic agonists [10–13]. However, all the data are in the range 4.8 Å [11] to 6.1 Å [13]. Thus, we have analysed the relationship of the r_{NN} distance with the thermodynamically most stable conformers for the protonated ABT-594. These conformers interconvert as a function of θ_2. Figure 7 collects the results for the r_{NN} distance as a function of the θ_2 angle. The θ_1 angle is kept fixed at 180°, and conformers VIII, V and II are included. We see that isoforms II and VIII, with $r_{NN} = 6.0$ Å, are within the range of r_{NN} values found in nicotinic agonists.

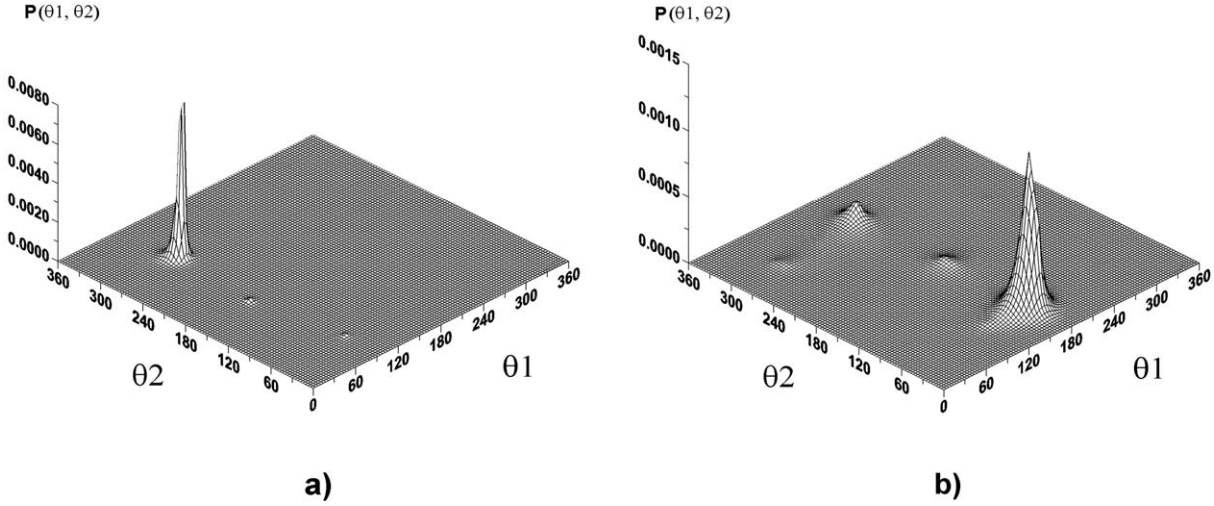

Figure 6. Wireframe map of conformational populations for neutral (case a), and protonated (case b) ABT-594 in solution at physiological temperature (37 °C). Angles in degrees.

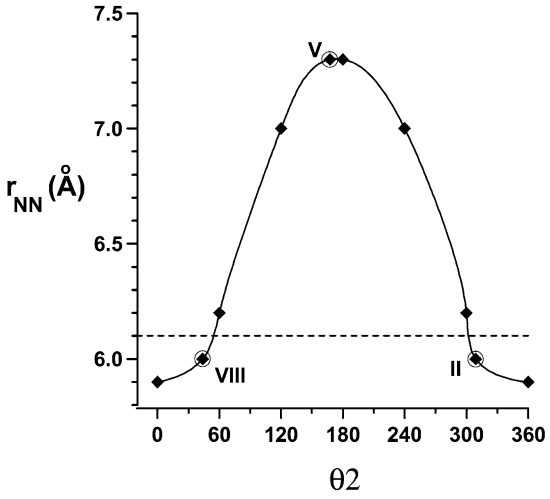

Figure 7. Internitrogen distance, r_{NN} (Å), as a function of the θ_2 dihedral in protonated ABT-594. Geometries optimized in vacuum. Isoforms II, V and VIII are included and indicated. The dashed line marks the upper limit of the range of r_{NN} distances for nicotinic agonists found in previous studies, $r_{NN} = 6.1$ Å.

On the other hand, isoform V with $r_{NN} = 7.3$ Å is outside the range by more than 1 Å. Thus, isoforms II and VIII are not only the preferred forms in solution, but also are candidates to be active conformations for binding to the nicotinic receptor. We can further analyse this point by considering the conformational behaviour when a given interaction energy comes into play. To simulate, qualitatively, the effect of the interaction energy, we consider the variation of population for a thermal bath with a kT factor higher than the one at physiological temperature (2.77 kJ mol^{-1}). Thus, we consider a kT factor of 8 kJ mol^{-1}. This value is high enough to affect the population, and see the trend of the change, but not so high as to populate indiscriminately all the minima. Figure 8 shows the resulting population for the protonated ABT-594 in solution. We observe that the population of isoforms V and especially II and VIII increases, with the peaks beginning to merge. Thus, it seems that the energy provided by interaction with the receptor permits easy rotation of the azetidinyl head between conformers II and VIII. In this form, adopting an optimal r_{NN} distance for binding to the receptor site is possible.

Conclusions

This work presents a study of the conformational behaviour and structural stability of the nicotinic analgesic ABT-594, (R)-5-(2-azetidinylmethoxy)-2-chloropyridine. Thus, we consider the neutral (precursor) and protonated (active) forms in vacuum and in aqueous solution.

Working at the MP2/cc-pVDZ level, a conformational analysis is performed on the two torsional angles describing the orientation of the azetidinyl group and the azetidinylmethoxy moiety. In vacuum and solution the same conformer (conformer I) is the most stable in the neutral form. Here, the nitrogen of the azetidinyl group is far from the electron pairs of the oxygen and from the pyridinic nitrogen. In the protonated form conformer VIII is the most stable in vacuum

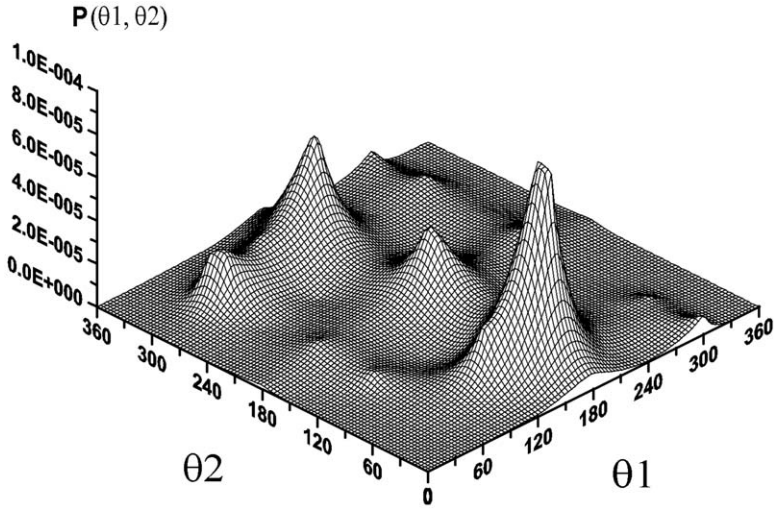

Figure 8. Wireframe map of conformational populations for protonated ABT-594 in solution in a thermal bath of kT=8 kJ mol^{-1}. Angles in degrees.

and solution. This conformer has the additional proton on the azetidinyl group oriented toward the electron lone pairs of the oxygen. For the neutral form, the effect of the solvent is to increase the barriers of interconversion between conformers. On the contrary, in the protonated form the solvent reduces the interconversion barriers. Thus, on energetic grounds, the active (protonated) form of ABT-594 is more flexible in solution.

To rationalize the structural stability of conformers I and VIII, we apply the atoms in molecules (AIM) theory. In the neutral form, conformer I is stabilized by an intramolecular hydrogen bond between the azetidinyl moiety and a hydrogen of the pyridinic ring. On the other hand, conformer VIII is stabilized by an intramolecular hydrogen bond between the oxygen and a hydrogen from one carbon of the azetidinyl group. The higher stability of conformer I is due to the higher strength of the hydrogen bond.

In the protonated form, conformer I stabilizes thanks to a cation-π interaction between the azetidinyl head and the pyridinic ring. In turn, conformer VIII also exhibits an intramolecular hydrogen bond between the oxygen and one hydrogen on the nitrogen of the azetidinyl group. The higher strength of this intramolecular hydrogen bond, over the cation-π interaction of conformer I, explains the higher stability of conformer VIII.

To account for entropic effects, we carried out a thermostatistical analysis of the population of each conformer at physiological temperature. It was found that conformer I is predominant in the neutral form. Its population increases when going from vacuum to solution. For the protonated ABT-594, conformer VIII is the most populated, although its population is reduced in solution. However, the closer conformer II (equivalent to conformer VIII by a torsion of the azetidinyl group) increases in population. Thus, in solution at physiological temperature, the active, protonated, form of ABT-594 is found in the conformational space limited by isoforms VIII and II.

The effect of the interaction energy with the receptor site on the conformational preferences of protonated ABT-594 was simulated by placing the molecule in a thermal bath for a kT factor of 8 kJ mol^{-1}. We observe that the effect is to populate the conformers associated to the rotation of the azetidinyl group. Thus, the interconversion between conformers VIII and II is favoured. In addition, we determined the internitrogen distance variation, which is one of the indices defining the nicotinic pharmacophore. It was found that only the zone corresponding to the interconversion of conformers VIII to II is placed within the boundaries of previously observed distances for nicotinic agonists. All these data suggest that the active conformation for the interaction of the protonated ABT-594 with the nicotinic receptor is within the conformational space delimited by conformers VIII to II.

Acknowledgements

The authors thank the Junta de Comunidades de Castilla-La Mancha (grant # PAI-02-001) for financial support.

References

1. MacPherson, R.D., Pharmacol. Therapeut., 88 (2000) 163.
2. Power, I. and Barrat, MsG., Surg. Clin. North. Am., 79 (1999) 275; Stalnikowicz, R. and Rachmilewitz, D., J. Clin. Gastroenterol., 17 (1993) 238.
3. Davis, L., Pollock, L.J. and Stone, T.T., Surg. Gynecol. Obstet., 55 (1932) 418.
4. Badio, B. and Daly, J.W., Mol. Pharmacol., 45 (1994) 563.
5. Daly, J.W., Garraffo, H.M., Spande, T.F., Decker, M.W., Sullivan, J.P. and Williams, M., Natural Products Reports, 17 (2000) 131.
6. Sullivan, J.P, Decker, M.W., Brioni, J.D., Donnelly-Roberts, D., Anderson, D.J., Bannon, A.W., Kang, C., Adams, P., Piattonikaplan, M., Buckley, M.J., Gopalakrishnan, M., Williams, M. and Arneric S.P., J. Pharmacol. Exp. Ther., 271 (1994) 624.
7. Spande, T.F., Garraffo, H.M., Edwards, M.W., Yeh, H.J.C., Pannell, L. and Daly, J.W., J. Am. Chem. Soc., 114 (1992) 3475.
8. Lloid, G.K. and Williams, M., Pharmacol. Exp. Ther., 292 (2000) 461.
9. Taylor, P. and Insel, P.A., Molecular basis of drug action, In: Pratt, W.B. and Taylor, P. (Eds.), Principles of Drug Action, third ed. Churchill Livingstone Inc., 1990, pp. 101–123.
10. Beers, W.H. and Earl, B.L., Nature, 228 (1970) 917.
11. Sheridan, R.P., Nilakantan, R., Dixon, J.S. and Venkataraghavan, R., J. Med. Chem., 29 (1986) 899.
12. Glennon, R.A., Herndon, J.L. and Dukat, M., Med. Chem. Res., 4 (1994) 461.
13. Abreo, M.A., Lin, N.H., Garvey, D.S., Gunn, D.E., Hettinger, A.M., Wasicak, J.T., Pavlik, P.A., Martin, Y.C., Donnelly-Roberts, D.L., Anderson, D.J., Sullivan, J. P., Williams, M., Americ, S.P. and Holladay, M.W., J. Med. Chem., 39 (1996) 817.
14. Glennon, R.A. and Dukat, M., Pharm. Acta Helv., 74 (2000) 103.
15. Decker, M.W., Meyer, M.D. and Sullivan, J.P., Expert Opin. Investig. Drugs, 10 (2001) 1819.
16. Holladay, M.W., Wasicak, J.T., Lin, N.H., He, Y., Ryther, K.B., Bannon, A.W., Buckley, M.J., Kim, D.J.B., Decker, M.W., Anderson, D.J., Campbell, J.E., Kuntzweiler, T.A., Donnelly-Roberts, D.L., Piattoni-Kaplan, M., Briggs, C.A., Williams, M. and Arneric, S.P., J. Med. Chem., 41 (1998) 407.
17. Bannon, A.W., Decker, M.W., Holladay, M.W., Curzon, P., Donnelly-Roberts, D., Puttfarcken, P.S., Bitner, R.S., Diaz, A, Dickenson, A.H., Porsolt, R.D., Williams, M. and Arneric, S.P., Science, 279 (1998) 77.
18. Donnelly-Roberts, D.L., Puttfarcken, P.S., Kuntzweiler, T.A., Briggs, C.A., Anderson, D.J., Campbell, J.E., Piattoni-Kaplan, M., McKenna, D.G., Wasicak, J.T., Holladay, M.W., Williams, M., and Arneric, S.P., J. Pharmacol. Exp. Ther., 285 (1998) 777.
19. Niño, A., Muñoz-Caro, C., Carbó-Dorca, R. and Girones, X., Biophys. Chem., 104 (2003) 417.
20. Dunning, Jr. T.H., J. Chem. Phys., 90 (1989) 1007.
21. Schlegel, H.B., J. Comput. Chem., 3 (1982) 214.
22. Cossi, M., Barone, V., Cammi, R. and Tomasi, J., Chem. Phys. Lett., 255 (1996) 327.
23. Barone, V., Cossi, M. and Tomasi, J., J. Chem. Phys., 107 (1997) 3210.
24. Frisch, M.J., Trucks, G.W., Schlegel, H.B., Scuseria, G.E., Robb, M.A., Cheeseman, J.R., Zakrzewski, V.G., Montgomery, J.A. Stratmann, R.E. Jr., Burant, J.C., Dapprich, S., Millam, J.M., Daniels, A.D., Kudin, K.N., Strain, M.C., Farkas, O., Tomasi, J., Barone, V., Cossi, M., Cammi, R., Mennucci, B., Pomelli, C., Adamo, C., Clifford, S., Ochterski, J., Petersson, G.A., Ayala, P.Y., Cui, Q., Morokuma, K., Malick, D.K., Rabuck, A.D., Raghavachari, K., Foresman, J.B., Cioslowski, J., Ortiz, J.V., Baboul, A.G., Stefanov, B.B., Liu, G., Liashenko, A., Piskorz, P., Komaromi, I., Gomperts, R., Martin, R.L., Fox, D.J., Keith, T., Al-Laham, M.A., Peng, C.Y., Nanayakkara, A., Gonzalez, C., Challacombe, M., Gill, P.M.W., Johnson, B., Chen, W., Wong, M.W., Andres, J.L., Gonzalez, C., Head-Gordon, M., Replogle, E.S. and Pople, J.A., Gaussian 98, Revision A.7, Gaussian, Inc., Pittsburgh, PA, 1998.
25. Cressie, N., Math. Geol., 22 (1990) 239; Oliver, M.A. and Webster, R., Int. J. Geogr. Inf. Systems., 4 (1990) 313; Cressie, N., Statistics for Spatial Data. John Wiley & Sons Inc., New York, 1993.
26. Surfer 8.0. Surface Mapping System. Golden Software Inc., 2002.
27. Farnell, L., Richards, W.G. and Ganellin, C.R., J. Theor. Biol., 43 (1974) 389; Richards, W.G., Quantum Pharmacology, Second Edition. Butterworth & Co., 1983; Grant, G.H. and Richards, W.G., Computational Chemistry. Oxford University Press, Oxford, UK, 1995.
28. Engeln-Müllges, G. and Uhlig, F., Numerical Algorithms with Fortran. Springer-Verlag, Berlin, Germany, 1996.
29. MORPHY98, a topological analysis program written by P.L.A. Popelier with a contribution from R.G.A. Bone, UMIST, Manchester, UK, 1998.
30. Barlocco, D., Cignarella, G., Tondi, D., Vianello, P., Villa, S., Bartolini, A., Ghelardini, C., Galeotti, N., Anderson, J., Kuntzweiler, T.A., Colombo, D. and Toma, L., J. Med. Chem., 41 (1998) 674.
31. Papke, R.L., Webster, J.C., Lippiello, P.M., Bencherif, M. and Francis, M.M., J. Neurochem., 75 (2000) 204.
32. Popelier, P., Atoms in Molecules. Prentice Hall, New York, 2000.
33. Bader, R.F.W., Atoms in Molecules. A Quantum Theory. Oxford University Press, Oxford, UK, 1995.
34. Takeshima, T, Fukumoto, R, Egawa, T. and Konaka, S., J. Phys. Chem. A, 106 (2002) 8734.
35. Muñoz-Caro, C. and Niño, A., Biophys. Chem., 96 (2002) 1.
36. Ma, J.C. and Dougherty, D.A., Chem. Rev., 97 (1997) 1303.